Building Gabor Filters from Retinal Responses

Johannes Partzsch, Christian Mayr and Rene Schuffny

Abstract— Starting from a biologically inspired framework, Gabor filters were built up from retinal filters via LMSE algorithms. A subset of retinal filter kernels was chosen to form a particular Gabor filter by using a weighted sum. One-dimensional optimization approaches were shown to be inappropriate for the problem. All model parameters were fixed with biological or image processing constraints. Detailed analysis of the optimization procedure led to the introduction of a minimization constraint. Finally, quantization of weighting factors was investigated. This resulted in an optimized cascaded structure of a Gabor filter bank implementation with lower computational cost.

Keywords— Gabor filter, image processing, optimization

I. INTRODUCTION

GABOR filters have desirable properties for picture analysis and feature extraction: They are selective in space, spatial frequency and orientation, achieving the theoretical limit for conjoint resolution in the spatial and spatial frequency domain ([1]). Therefore, they have been widely used in these fields in recent years ([2], [3], [4]). Those filters were also used to describe the behavior of simple cells in area V1 of the human visual cortex, which has turned out to be very successful ([5]). It is thus worth going back to the roots and taking a look on how Gabor filters are composed in nature.

The human retina gathers optical information about the environment via its 10^8 photoreceptors. Horizontal, bipolar and amacrin cells filter the information, and the 10^6 ganglion cells code the filter outputs into spike trains, sending them to the optic nerve. In this process, a lot of information compression is needed ([6], [7]) due to the relatively few number of outputs. To achieve this, the overall retinal filtering consists of lowpass and bandpass filtering, emphasizing changes in illumination and suppressing regions with uniform brightness. The next processing stage in the human visual system is area V1 of the visual cortex. There, basic features of the image are extracted by combining retinal outputs, so that overall Gabor-like receptive fields arise ([8]).

The idea of building Gabor filters from retinal responses is not new; it was already stated by Thiem et al. ([9], [10]). We use their principal idea of building Gabor filters by linearly combining outputs of retinal filters, using least mean square error (LMSE) optimization. In contrast to their emphasis on the system's archictecture and the hexagonal sampling, we here investigate the optimization process in more detail. This includes adjusting the retinal filter parameters, analysing and

extending the standard LMSE optimization, and testing the influence of quantised weighting factors on the optimization results. In particular, we show that one-dimensional optimization approaches are insufficient for the problem, and introduce a minimization equation leading to a far better weighting factor distribution. The latter is a prerequisite for successfully quantising the weights. From the quantisation results, we propose a simplified cascaded structure for Gabor filter banks compared to that introduced in [10], and compare the computational cost of the approach with standard Gabor filter bank implementations.

In section II, we develop a model for the retinal filters. Section III will introduce a Gabor filter model and describe and analyse the different optimization procedures. Finally, section IV shows how quantization of coefficients influences the results and describes the simplified cascaded structure of a Gabor filter bank.

II. MODEL OF THE RETINA

In a simple approach, the retina as a whole can be seen as performing a discrete convolution of the input image with a retinal filter kernel. In other words, it could be modeled by a discrete, linear filter. Each output of a ganglion cell represents the filter output at a particular position, coded in a spike train.

The retinal filter kernels have a center-surround structure, i.e. center and surround have opposite sign (see [11], for example). As negative filter outputs are hard to code into a spike train by retinal ganglion cells, there exist cell pairs for each filter output: The so-called ON-center cell codes the positive values, and the OFF-center cell codes the negative values using a negated filter kernel ([12]).

A common model for the filter kernels is the Difference-of-Gaussian (DoG) model. It consists of two Gaussians with different variances and can generally be written as

$$d(x,y) = a_1 \cdot e^{-\frac{x^2+y^2}{2\sigma_1^2}} - a_2 \cdot e^{-\frac{x^2+y^2}{2\sigma_2^2}} . \qquad (1)$$

In our model, the filter will be pure bandpass, meaning that uniform brightness will be generating zero filter output. To ensure this, the integral over the filter kernel has to be zero as well. Because the overall amplitude of the DoG has no influence on the analysis and is adjusted later by the coefficients used to combine the retinal filter kernels to Gabor filters, we simply set the maximum of the first Gaussian to 1. Then we receive the form

$$d(x,y) = e^{-\frac{x^2+y^2}{2\sigma_1^2}} - \frac{1}{a^2} \cdot e^{-\frac{x^2+y^2}{2a^2\sigma_1^2}} , \text{ with } a = \frac{\sigma_2}{\sigma_1} . \quad (2)$$

Whereas σ_1 fixes the spatial size of the filter kernel, a defines its shape. In contrast to what results of biological experiments

suggest (e.g. [12]), we will not vary a in our model, because it is not thought to be biologically exact but aims for efficient signal processing. According to [13], we choose $a = 1, 6$ to approximate the Laplacian-of-a-Gaussian(LoG) model, which was also used by [10]. The retinal filter according to this value is shown in picture 1A.

To fix the value of σ_1, we consider the Fourier transform of the DoG, which is

$$D(u,v) = 2\pi\sigma_1^2 \cdot \left(e^{-2\sigma_1^2(u^2+v^2)} - e^{-2a^2\sigma_1^2(u^2+v^2)} \right) \quad . \quad (3)$$

As can be seen in figure 1C, the DoG behaves like a bandpass filter with the mid frequency proportional to $\frac{1}{\sigma_1}$. The Gabor filter is also bandpass, so a constraint on σ_1 is that the frequency range of the DoG filters lies within the frequency range of the Gabor filter. After introducing Gabor filtering in the next section, we will describe this a bit more precisely.

Fig. 2. Gabor function: A: shapes of real (dashed line) and imaginary(dotted line) part in x-direction. B,C: real and imaginary part as 2D profile. D: spectrum in u-direction(solid line), and spectra of real(dashed) and imaginary(dotted) part. E: 2D profile of the Gabor spectrum. F: 2D profile of the Fourier transformed real part.
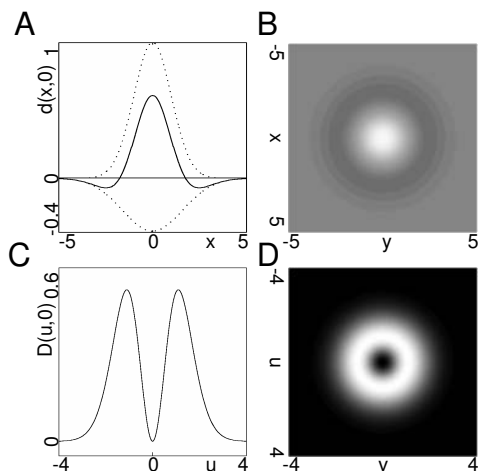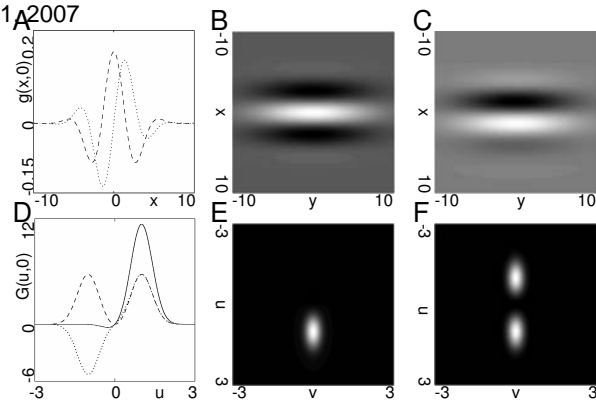

Fig. 1. DoG filters: A: composition of the DoG function out of two Gaussians. B: 2D-profile, corresponding to an ON-center ganglion cell. C,D: spectrum of the DoG function in 1D and 2D. Shape parameter $a = 1.6$ and standard deviation $\sigma_1 = 1$ for all charts.

III. SYNTHESIS OF GABOR FILTERS

Before starting to compose Gabor filters, we have to describe them mathematically. Lee ([1]) has derived a Gabor filter model that is based on biological experiments, but also considers constraints from information processing, such as zero mean or L^2 normalization. It has the form

$$g(x,y) = \frac{\omega_0}{\sqrt{\pi d} \cdot k} \cdot e^{-\frac{\omega_0^2}{2k^2}(x^2+\frac{y^2}{d^2})} \cdot \left(e^{j\omega_0 x} - e^{-\frac{k^2}{2}} \right) \quad (4)$$

and its spectrum is given by

$$G(u,v) = 2\sqrt{\pi d}\frac{k}{\omega_0} \cdot e^{-\frac{k^2 d^2}{2\omega_0^2}v^2} \quad (5)$$
$$\cdot \left(e^{-\frac{k^2}{2\omega_0^2}(u-\omega_0)^2} - e^{-\frac{k^2}{2}} \cdot e^{-\frac{k^2}{2\omega_0^2}u^2} \right) \quad .$$

Both the filter and its spectrum are displayed in figure 2.

As the filter function is complex, real and imaginary part have to be treated separately. In fact, simple cells in V1 are arranged in pairs, with each pair approximately having

a quadrature characteristic ([1], [14]). The Gabor function consists of a two-dimensional elliptic Gaussian, spreading along the y-axis, and a zero-mean complex oscillation along the x-axis. Its spatial size and spatial mid-frequency can be adjusted by ω_0, whereas the parameter k defines the spatial frequency bandwidth and d the length-to-width-ratio of the elliptic Gaussian. According to [1], we choose $d = 2$ and a bandwidth of 1.5 octaves, which corresponds to $k = 2.5$. For different orientations of the Gabor filter, the local filter coordinates (x,y) have to be rotated with respect to the global image coordinates.

Now that we have described the Gabor filter kernels, we can start composing them from retinal DoG filters. Like Thiem et al. ([9]), we use a linear approach:

$$g(x,y) \approx \sum_{(j)} a_j \cdot d_{\sigma_j}(x,y) \quad , \quad (6)$$

where d_{σ_j} is the DoG kernel with standard deviation $\sigma_1 = \sigma_j$. The coefficients a_j have to be determined by an optimization procedure. This can be done by defining a set of control points (x_i, y_i). For each control point, (6) defines one equation of a linear system of equations. For good optimization results, there should be far more control points (x_i, y_i) than coefficients a_j; we used 10 times more control points than coefficients. The resulting overdetermined system of equations can be solved in a least mean square error (LMSE) sense.

One of the noteworthy properties of the Gabor filter is cartesian separability, i.e. the possibility to separate the function into a product $g(x,y) = g_1(x) \cdot g_2(y)$, where x and y are oriented along the main axes of the Gabor function. This property was also found in receptive fields of V1 simple cells (see [8]). It could be used to simplify the optimization from a 2-dimensional problem into two 1-dimensional problems. A prerequisite for this method is cartesian separability of the basis functions, which is not the case for DoG-functions. So our results would suffer from an additional systematic error. Even when using another, cartesian separable approximation of a retinal filter kernel, there is a further drawback: The solution would lead to a rectangular grid of retinal cells,

oriented along the main axes of the Gabor filter. So one would have to choose whether to take a grid of retinal cells for each desired orientation of Gabors (there is at best a re-use of a grid for the 90°-rotated filters), which would be very inefficient, or whether to take a single grid and then use for each required retinal cell the nearest available position, which would likely be highly inaccurate or (if the grid was fine) again very inefficient. For this reasons, the 1D-approach is unsuitable for the problem.

With a more general 2D-approach, the positions of retinal filter cells can be chosen arbitrarily. For simplicity, we will use quadratic grids of retinal filter cells with different statial and spatial frequency size, i.e. different σ_1. A hexagonal grid would be more efficient in terms of the sampling theorem and is approximately used in the retina of mammals and humans ([9]), but that would be incompatible with common image processing and quadratically sampled digital images. Furthermore, the density of photoreceptors and ganglion cells in the retina is not constant ([13]), so a uniform grid can only be a coarse, local approximation to the arrangement in a human retina.

To determine the σ_1, we consider the spectra of DoG and Gabor, shown in figures 1 and 2. As mentioned, the frequency range of the DoG filter has to be within the frequency range of the Gabor. Especially the maximum of the DoG amplitude spectrum has to lie inside the Gabor spectrum. To express this, we use the amplitude of frequency $r = \sqrt{u^2 + v^2}$. As the DoG spectrum is radially symmetric, it becomes a 1-dimensional function $D(r)$:

$$D(r) = 2\pi\sigma_1^2 \cdot \left(e^{-2\sigma_1^2 r^2} - e^{-2a^2\sigma_1^2 r^2} \right) \qquad (7)$$

with maximum at:

$$r_{max} = \frac{1}{\sigma_1} \cdot \sqrt{\frac{\ln a}{a^2 - 1}} \approx \frac{0.55}{\sigma_1} \quad (a = 1.6) \ . \qquad (8)$$

For describing the extent of the Gabor spectrum, we adopt a typical estimation from statistics for Gaussian distributions: We calculate the amplitude maximum $(\bar{u}, \bar{v})$ in the frequency domain and take the standard deviations σ_u and σ_v as a measure for the expansion of the spectrum. In the following, we will separately derive espressions for the u- and v-direction. As the Gabor function is a single Gaussian in the v-direction, we can simply read off its mean and standard deviation:

$$\bar{v} = 0 \ , \quad \sigma_v = \frac{\omega_0}{kd} \ . \qquad (9)$$

Deriving the maximum in the u-direction is a bit more complicated. The part of the spectrum dependent on u is given by:

$$G_1(u) = e^{-\frac{k^2}{2\omega_0^2}(u-\omega_0)^2} - e^{-\frac{k^2}{2}} \cdot e^{-\frac{k^2}{2\omega_0^2}u^2} \ . \qquad (10)$$

The derivation of this function has to be set to zero, yielding a nonlinear equation that has to be solved:

$$\frac{1}{z} + e^{-k^2 z} - 1 = 0 \ , \ z = \frac{\bar{u}}{\omega_0} \ \rightarrow \ z \approx 1 \text{ for } k = 2.5 \ . \qquad (11)$$

The standard deviation is simply taken from the two Gaussian functions in $G_1(u)$, giving as result for the u-direction:

$$\bar{u} = \omega_0 \ , \quad \sigma_u = \frac{\omega_0}{k} \ . \qquad (12)$$

Then we calculate the r-frequency range when taking the $n \cdot \sigma_u$ and $n \cdot \sigma_v$- interval:

$$\sqrt{0^2 + \omega_0^2(1 - \frac{n}{k})^2} \leq r \leq \sqrt{(\frac{n\omega_0}{kd})^2 + \omega_0^2(1 + \frac{n}{k})^2} \ , \qquad (13)$$

which, with formula (8), yields

$$n = 1 : \quad \frac{0.39}{\omega_0} \leq \sigma_1 \leq \frac{0.92}{\omega_0} \qquad (14)$$

$$n = 2 : \quad \frac{0.29}{\omega_0} \leq \sigma_1 \leq \frac{2.75}{\omega_0} \ . \qquad (15)$$

This is a relatively wide range, because we have only used the maximum of the DoG function and ignored its frequency range.

We will use octave sampling here, i.e. increasing σ_1 by a factor of 2 for subsequent grids, and change the width of the grid accordingly:

$$\sigma_{1,m} = \sigma_{1,0} \cdot 2^m \ , \quad \Delta x_m = \Delta x_0 \cdot 2^m \ , \ 0 \leq m \leq M - 1 \ , \qquad (16)$$

where M is the number of grids/octaves. To limit the number of DoG functions, we only use those, whose center (x_0, y_0) lies inside a circular area around the center of the Gabor filter mask. The radius of this area is proportional to the size of the Gabor major axis:

$$x_0^2 + y_0^2 \leq R^2 \ , \quad R = \alpha_R \cdot \frac{kd}{\omega_0} \ . \qquad (17)$$

Simulations with different α_R show, that $\alpha_R = 1.5$ gives a good trade-off between accuracy at the boundary and number of DoG masks.

Figure 3 shows simulation results for different orientations. Because the quadratic grids are highly symmetric, we only need to consider Gabor filters for orientations $0 \leq \phi \leq 45°$, all others can be obtained by mirroring at one of the symmetry axes. We will use $\omega_0 = 1$ for all simulations without loss of generality, because all parameters are fixed relative to ω_0. Furthermore, we will only show simulations for the real part of the Gabor function, as the results for the imaginary part are similar.

The synthesized Gabor filters look very similar to the original ones, exept that they are a bit compressed at the ends of their main axis. In figure 3 E,F , a test image was filtered with the masks shown in figure 3 B and C. Again, the results look very similar. When we increase the grid width, the number of DoG masks decreases, but the results get worse. For $\Delta x = 2\sigma_1$, the shape of the filter changes significantly, whereas the filtered image still looks rather the same (Fig. 4 B). With higher grid widths, the results get useless, because the DoG masks overlap little (Fig. 4 C). When increasing $\sigma_{1,0}$, the masks first stay very much the same, either with or without increasing the grid width (Fig. 4 D and E). But for values $\sigma_{1,0} > \frac{2}{\omega_0}$, either the system of equations gets rank deficient, or there appear undesired bumps in the outer regions of the mask, which make the filtering results useless. Seen overall, the frequency range calculated at the beginning of this section is too wide, but gives a reasonable starting point.

Let us now examine the histograms. There is no reason for the few high values of the a_j, which are likely to be the
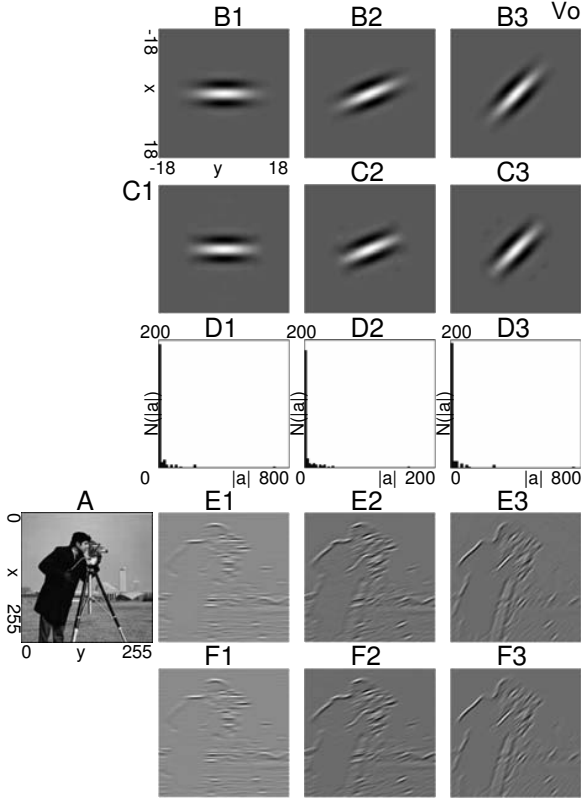
Fig. 3. Original and synthesized Gabor filters for different orientations: 0°
(1), 22.5° (2) and 45° (3). Parameters are: $\sigma_{1,0} = \frac{1}{\omega_0}$, $\Delta x_0 = \sigma_{1,0}$, M=3
octaves, leading to N=231 DoG masks. A: test image; B: Gabor filters derived
from equation (4); C: composed filters; D: histograms of weighting factors a_j,
amplitudes sorted into 50 equally spaced bins (note the few very high values
distorting the histograms); E: image A filtered with Gabor kernels shown in
B; F: image A filtered with approximated masks shown in C. (Axes for E,F
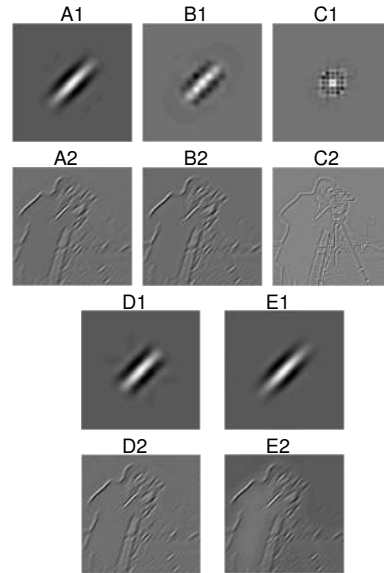as in A; for B,C as in B3)

Fig. 4. Parameter variation: 1: synthesized filter masks, 2: results of test
image filtering. A: $\sigma_{1,0} = \frac{1}{\omega_0}$, $\Delta x_0 = \sigma_{1,0}$. B: $\sigma_{1,0} = \frac{1}{\omega_0}$, $\Delta x_0 = 2\sigma_{1,0}$.
C: $\sigma_{1,0} = \frac{0.5}{\omega_0}$, $\Delta x_0 = 3\sigma_{1,0}$. D: $\sigma_{1,0} = \frac{2}{\omega_0}$, $\Delta x_0 = 0.5\sigma_{1,0}$. E: $\sigma_{1,0} = \frac{2}{\omega_0}$, $\Delta x_0 = \sigma_{1,0}$. (Axes as in Fig. 3)
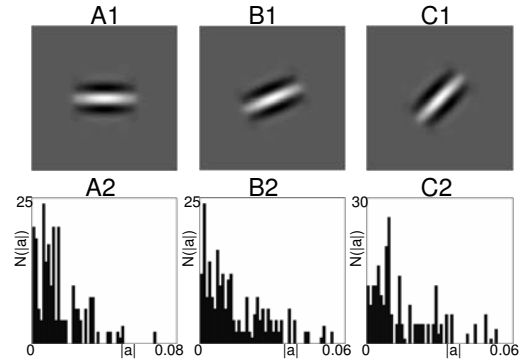

Fig. 5. Results of minimization: synthesized Gabor filters with orientation
0°(A), 22.5° (B) and 45° (C). 1: filter masks. 2: histograms. Same conditions
and axes as in Fig.3 .

result of numerical side effects. This problem could be solved
by introducing an additional minimization condition, using a
sum of squares:

$$\sum_{(j)} a_j^2 \rightarrow \min \quad . \tag{18}$$

The LMSE-solution of this nonlinear system of equations
gives as good results as without minimization, but with far
better distribution of coefficients, as figure 5 shows. Such an
additional minimization equation should therefore be included
into optimization problems like this one.

IV. QUANTIZATION

We will now investigate the effects of quantized coefficients
on the results of the composition. Those depend on how strong
deviations from the optimal solution worsen the filter masks.
We quantize the amplitudes of the coefficients in K equal
intervals relative to a maximum value, so the allowed values
are:

$$a_{\pm k} = \pm \frac{k}{K-1} \cdot a_{max} \quad , \quad k = 0, 1, \ldots, K-1 \quad . \tag{19}$$

For optimal results, we use a successive approximation proce-
dure. First, the full overdetermined system of equations as in

equation (6) is solved, including minimization of coefficients
(equation (18)), since a narrow range of values is necessary for
good quantization. Then a_{max} is determined slightly smaller
than the maximal occurring amplitude ($a_{max} = 0.95|a|_{\max}$).
Thereafter, all coefficients that are in a range ϵ around an
allowed value are fixed to that value, and the system of
equations is solved for the remaining non-fixed a_j. This
procedure is continued, increasing the range ϵ subsequently,
until all coefficients are fixed to an allowed value.

Figure 6 A-C shows results for the standard case (figure 3).
The masks look slightly different, with some jitter occurring at
the outer regions, which, however, does not affect the filtering
results. So, even when only switching on and off DoG masks
without any weighting factor (except the sign) as shown in
C, the results become not significantly worse. This is an
indication for the robustness of the synthesis process.

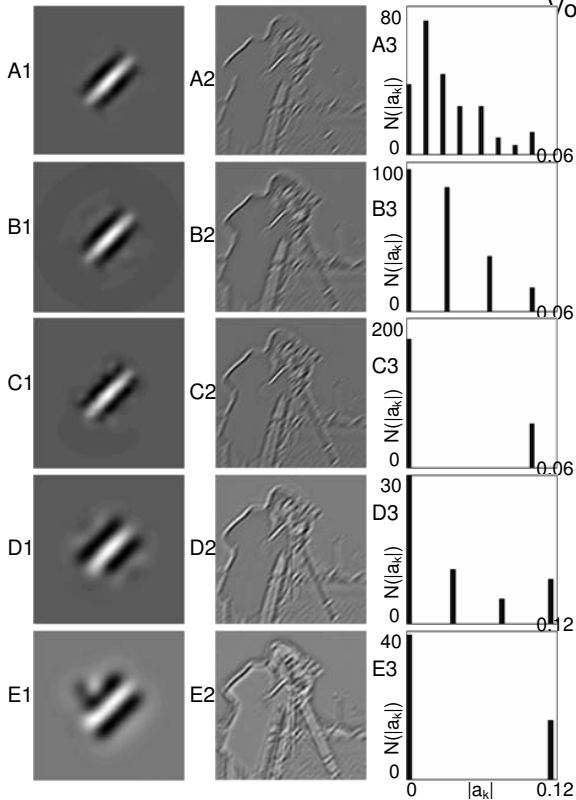To test the limits of the method, we repeat the quantization

Fig. 6. Results for quantized coefficients. 1: synthesized filter masks, 2: results of test image filtering, 3:histogram. In A-C, parameters $\sigma_{1,0} = \frac{1}{\omega_0}$, $\Delta x_0 = \sigma_{1,0}$ are used and K is set to 8 (A), 4 (B) and 2 (C). D and E show data for $\sigma_{1,0} = \frac{2}{\omega_0}$, $\Delta x_0 = \sigma_{1,0}$. In D, $K = 4$ and in E, $K = 2$, leading to poorer results. Conditions and axes are the same as in Fig. 3, except the bin count of 30 for the histograms.
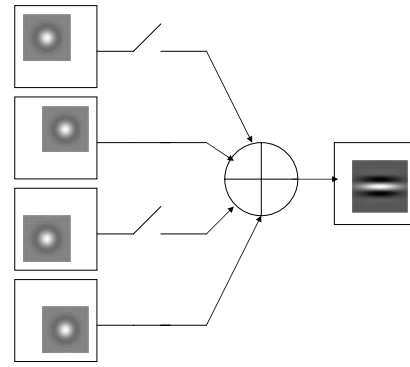

Fig. 7. Cascaded filter structure: For calculating the Gabor filter output at a particular position, selected DoG-filter outputs are added together.

combination of DoG masks is then stored for subsequent filterings.

For showing the advantage of the approach described above, let us compare the computational cost with a standard Gabor filter bank. In the standard approach, a discrete convolution is calculated for each desired Gabor filter. Assuming a number of N_G Gabor filters, an (output) image size of $X \cdot Y$ pixels and a size of the filter kernel of $U \cdot V$ pixels, filtering an image would require approximately $N_G \cdot X \cdot Y \cdot U \cdot V$ multiplications and the same number of additions. The approach with composed Gabor filters requires to calculate discrete convolutions for each of the N_R retinal DoG-layers with approximately $N_R \cdot X \cdot Y \cdot U \cdot V$ multiplications and additions. One could argue that the filter kernel size varies from layer to layer, but this is compensated by the coarser sampling of DoG filters with greater spatial extent. The composition of the Gabor filter approximation requires M_G additions for each position, which leads to $N_G \cdot X \cdot Y \cdot M_G$ additions for the whole sampling process. The difference between standard Gabor filter bank and composed-Gabor filter bank is then

$$\Delta C = N_G \cdot X \cdot Y \cdot \left[U \cdot V \cdot \left(1 - \frac{N_R}{N_G}\right) - M_G \right] . \quad (20)$$

For a big filter bank, the approximation $N_R \ll N_G$ holds, so the term in brackets simplifies to $[U \cdot V - M_G]$. For practical filter sizes, $U \cdot V$ is much bigger than M_G. In the figures presented in this paper, $U = V = 16$ was used, which leads to a reduction of computational cost of factor 5 for the first quantisation (with ca. 50 coefficients unequal to zero) and of factor 16 for the arrangement with fewer DoG masks. Note that we combined multiplication and addition to one operation and thus did not take the reduced computational costs due to the missing multiplications in case of the composed-Gabor filter bank into account.

V. CONCLUSION

In this paper, a model for the retinal filter kernels has been developed inspired by experimental results and image processing methods. In a biology-inspired approach, Gabor filters were composed from the retinal filters using LMSE-algorithms. Therefore, parameters of the DoG filters were fixed

for an arrangement with fewer DoG masks (figure 4 E). Here, the results become significantly worse for strong quantization, as can be seen from figure 6 D,E, but could still be used as a reasonable approximation of a Gabor filter. Notice that there are only 16 coefficients unequal to zero in the last case (see height of bar at 0.12 in figure 6 E).

This small number of DoG masks needed to form a reasonable Gabor filter could be used for an efficient implementation of a Gabor filter bank, using a cascaded structure as was mentioned in [10]. Instead of calculating a convolution for each Gabor filter - which is computationally expensive and has caused efforts in developing optimization strategies reducing the size of filter banks ([16], [15]) - the convolution is only calculated for a few DoG masks (3 in our case), and for each position there only needs to be added a certain set of filter outputs together to form an approximation of a particular Gabor filter (see figure 7). This goes beyond the approach of [10], where filter outputs are weighted before summation. Calculating another Gabor filter would only require to sum up another set of DoG filter outputs, but would avoid the computation of a convolution. This method requires a pre-calculation, which is much more expensive than a convolution, as there have to be solved several overdetermined, nonlinear systems of equations. But this can be done once, and the

relative to the Gabor masks and methods with separate 1-dimensional composition were proven to be insufficient to the problem. The composed masks are very similar to the original Gabor filters and it was shown that they are relatively insensible to parameter variations. To optimize the amplitudes of the coefficients, an additional minimization equation was used, which dramatically improved the distribution of amplitudes. Finally, the effects of quantization of coefficients were investigated with no significant worsening of results. This leads us to the conclusion, that an "all-or-nothing" approach, despite its coarse quantization can yield accurate Gabor filter masks. Inspired by the results, we propose an efficient implementation of a Gabor filter bank, which could enable the use of a high number of filters with relatively low computational expense.

Composition of Gabor filters could in principle be done with localized filters other than DoG filters, which would be maybe as efficient as with DoG filters or yield even better results. In this paper, we have restricted ourselves to a biological framework, for which filters similar to DoG filters are necessary to reproduce retinal behavior. Testing our approach with other filter kernels would be very interesting in that it helps assessing the results of composition with DoG filters. Furthermore, the composition of a large number of filters from a few basis filters could be a useful strategy for the efficient implementation of filter banks in general.

REFERENCES

[1] Lee, T.S. (1996): *Image Representation Using 2D Gabor Wavelets*, IEEE Transactions on Pattern Analysis and Machine Intelligence, Vol. 18, Issue 10, pp. 951-979

[2] Xu, Y., Zhang, X. (2005): *Gabor Filterbank and its Application in the Fingerprint Texture Analysis*, PDCAT 2005, pp. 829-831

[3] Huang, L., Shimizu, A., Kobatake, H. (2004): *Classification-Based Face Detection Using Gabor Filter Features*, Proceedings to the 6. IEEE International Conference on Automatic Face and Gesture Recognition, pp. 397-402

[4] Jain, A.K., Prabhakar, S., Hong, L., Pankanti, S. (2000): *Filterbank-Based Fingerprint Matching*, IEEE Transactions on Image Processing, Vol. 9, Issue 5, pp. 846-859

[5] Jones, J.P., Palmer, L.A. (1987): *An Evaluation of the Two-Dimensional Gabor Filter Model of Simple Receptive Fields in Cat Striate Cortex*, Journal of Neurophysiology, Vol. 58, Issue 6, pp. 1233-1258

[6] Van Essen, D.C., Anderson, C.H. (1995): *Information Processing Strategies and Pathways in the Primate Visual System* in: An Introduction to Neural and Electronic Networks, 2nd ed., Academic Press, Zornetzer et. al., eds., pp. 45-76

[7] Meister, M., Berry, M.J. (1999): *The Neural Code of the Retina*, Neuron, Vol. 22, pp. 435-450

[8] Jones, J.P., Palmer, L.A. (1987): *The Two-Dimensional Spatial Structure of Simple Receptive Fields in Cat Striate Cortex*, Journal of Neurophysiology, Vol. 58, Issue 6, pp. 1187-1211

[9] Thiem, J., Wolff, C., Hartmann, G. (2000): *Biology-Inspired Early Vision System for a Spike Processing Neurocomputer*, Lecture Notes In Computer Science, Vol. 1811, pp. 387-396

[10] Thiem, J., Hartmann, G. (2000): *Biology-inspired Design of Digital Gabor Filters upon a Hexagonal Sampling Scheme*, Proceedings of the 15th International Conference on Pattern Recognition

[11] Merwine, D.K., Amthor, F.R., Grzywacz, N.M. (1995): *Interaction between center and surround in rabbit retinal ganglion cells*, Journal of Neurophysiology, Vol. 73, Issue 4, pp. 1547-1567

[12] Dacey, D., Packer, O.S., Diller, L., Brainard, D., Peterson, B., Lee, B. (2000): *Center surround receptive field structure of cone bipolar cells in primate retina*, Vision Research, Vol. 40, pp. 1801-1811

[13] Balasuriya, L. S., Siebert, J. P. (2003): *A low level vision hierarchy based on an irregularly sampled retina*, Proceedings of the International Conference on Computational Intelligence, Robotics and Autonomous Systems, Singapore, December 2003

[14] Daugman, J.G. (1993): *Quadrature-phase simple-cell pairs are appropriately described in complex analytic form*, Journal of the Optical Society of America A, Vol. 10, Issue 2, pp. 375-377

[15] Sun, Z., Bebis, G., Miller, R. (2005): *On-road vehicle detection using evolutionary Gabor filter optimization*, IEEE Transactions on Intelligent Transportation Systems, Vol. 6, Issue 2, pp. 125-137

[16] Weldon, T.P., Higgins, W.E., Dunn, D.F. (1995): *Gabor filter design for multiple texture segmentation*, Optical Engineering Vol. 35, Issue 10, pp. 2852-2863